Effect of Multiple Aliphatic Amino Acids Substitutions on the Structure, Function, and Mode of Action of Diastereomeric Membrane Active Peptides

Dorit Avrahami,[‡] Ziv Oren,[‡] and Yechiel Shai*[,§]

Department of Biological Chemistry, Weizmann Institute of Science, Rehovot, 76100 Israel

Received March 15, 2001; Revised Manuscript Received August 13, 2001

ABSTRACT: The initial stages leading to the binding and functioning of membrane-active polypeptides including hormones, signal sequences, and lytic peptides are mainly governed by electrostatic attraction and hydrophobic partitioning between water and lipid bilayers. Antimicrobial peptides serve as an important model for studying the details of these initial steps. However, a systematic analysis of the contribution of multiple hydrophobic amino acids to these steps have been hindered by the propensity of many peptides to aggregate and become inactivated in solution. To this end, we synthesized a series of model amphipathic all L-amino acid peptides and their diastereomers with the sequence $KX_3KWX_2KX_2K$, where X = Gly, Ala, Val, Ile, or Leu. The effect of the aliphatic amino acids on the biological activity, binding, structure, membrane localization, and mode of action of these peptides was investigated. Most of the L-amino acid peptides oligomerized and adopted distinct structures in solution and in a membrane mimetic environment. Among this group only the Leu containing peptide was hemolytic and highly active on most bacteria tested. The Val- and Leu-containing peptides were hemolytic but inactive toward most bacteria tested. In contrast, the diastereomeric peptides were monomeric and unstructured in solution, but they adopted distinct structures upon membrane binding. While hemolytic activity was drastically reduced, the spectrum of antibacterial activity was preserved or increased. Importantly, we found a direct correlation with the diastereomers between hydrophobicity and propensity to form a helical/distorted-helix and activity (induced membrane leakage and antibacterial activity), despite the fact that they contained 30% D-amino acids. Furthermore, efficient increase in membrane permeability can proceed through different mechanisms. Specifically, the Leu-containing diastereomeric peptide micellized vesicles and possibly bacterial membranes while the Ile-containing diastereomeric peptide fused model membranes and irregularly disrupted bacterial membranes.

Electrostatic attraction and hydrophobic partitioning were shown to act concertedly to promote the initial stages leading to the binding of membrane active polypeptides including hormones, signal sequences, and cytolytic peptides. Antimicrobial peptides have served as an important model for these studies (reviewed in refs *1*−*5*). A major group within this family is positively charged, amphipathic, α-helical peptides that are able to increase phospholipid membranes permeability. A net positive charge facilitates initial binding, through an electrostatic interaction, to the negatively charged bacterial membrane. Increased membrane permeability follows, which is governed by the hydrophobic portion of the peptide. Understanding and predicting the membrane activity of antimicrobial peptides requires quantifying the contribution of individual hydrophobic amino acids to peptide structure, membrane binding and increasing membrane permeability activity, without altering other physicochemical properties.

A major effort has been made to quantify the hydrophobicity of a single amino acid by measuring its partitioning between water and lipid bilayers or between water and an organic phase, resulting in a comprehensive listing of hydrophobic indices (*6*−*10*). In addition, a complete interfacial hydrophobicity scale that includes the contribution of the peptide bond was presented by Wimley and White (*11*), who, using a series of "host−guest" pentapeptides, determined the free energies of transfer of each amino acid side chain between water and the bilayer interface. In other studies, Shin and co-workers (*12*, *13*) introduced uncharged amino acids individually at a guest site in α-helical membrane binding peptides and measured their partitioning into phospholipid membranes. However, comparative studies using substitution of several amino acids at once in long peptides is more complicated due to major changes in physicochemical properties of the resultant analogues. The effect of hydrophobic amino acids on the secondary structure in the membrane is different from its effect in solution. For example, it was shown that the bilayer significantly promotes the helix formation of C_β-branching residues such as Val and Ile in transmembrane helices (*14*−*16*). Furthermore, different hydrophobic amino acids affect the aggregation of the peptides in solution and in membranes. Once a face on

[†] This research was supported by the Israel Academy of Sciences and Humanities.

* To whom correspondence should be addressed. Phone: 972-8-9342711. Fax: 972-8-9344112. E-mail: Yechiel.Shai@ weizmann.ac.il.

[‡] These authors contributed equally to the paper.

[§] The Harold S. and Harriet B. Brady Professorial Chair in Cancer Research.

10.1021/bi0105330 CCC: $20.00
Published on Web 09/29/2001

an amphipathic α-helical peptide is hydrophobic enough to yield substantial membrane binding, it is usually hydrophobic enough to also induce oligomerization in aqueous solution (*17*). Moreover, self-association in solution limits peptide solubility and modifies the interactions with membranes, consequently leading to a decrease in biological function (*17*).

Previous studies revealed that the replacement of few L-amino acids with their D-enantiomers in the amphipathic helical peptides pardaxin (*18*, *19*), melittin (*20*), magainin (*21*), and short-model peptides composed of leucine and lysine preserved their ability to bind and increase membrane permeability of negatively charged phospholipid membranes, thus maintaining their functional structures. For example, a NMR study of the structure of a melittin diastereomer revealed an amphipathic α-helix in the C-terminal region of the diastereomer in TFE/water, methanol, and in DPC/DMPG micelles, similar to native melittin (*22*). Furthermore, in an ATR-FTIR spectroscopy study, a structure of ~90% α-helix was manifested in a short model diastereomer composed of leucine and lysine incorporated into lipid bilayers, despite a composition of 33% D-amino acids (*23*). Notably, the diastereomer was a monomer in solution compared to an oligomer formed by the parental L-amino acid peptide.

Here we examined the effect of multiple substitutions of different hydrophobic aliphatic amino acids to the structure, membrane binding, and biological function of diastereomeric peptides. For this purpose, we synthesized a group of peptides having a sequence $KX_3KWX_2KX_2K$ where X = Gly, Ala, Val, Ile, or Leu. For each sequence (besides K_4G_7W), all L-amino acids and their diastereomers (four L-amino acids were substituted with their D-enantiomers) were synthesized and analyzed. The results are discussed in relation to the contribution of the different aliphatic amino acids to the binding, structure, and depth of penetration into the membrane, with ramifications regarding the molecular mechanism by which this group of peptides kills bacteria and lyses erythrocytes.

MATERIALS AND METHODS

Materials. 4-Methyl benzhydrylamine resin (BHA) and butyloxycarbonyl (Boc) amino acids were purchased from Calibochem-Novabiochem (La Jolla, CA). The following protecting groups were used: formyl (For) for tryptophan and 2-chlorobenzyloxycarbonyl (2-Cl-Z) for lysine. Other reagents used for peptide synthesis included trifluoroacetic acid (TFA, Sigma), *N*,*N*-diisopropylethylamine (DIEA, Aldrich, distilled over ninhydrin), dicyclohexylcarbodiimide (DCC, Fluka), 1-hydroxybenzotriazole (HOBT, Pierce), and dimethylformamide (peptide synthesis grade, Biolab). Egg phosphatidylcholine (PC) was purchased from Lipid Products (South Nutfield, U.K). Egg phosphatidylglycerol (PG), and phosphatidylethanolamine (PE) (Type V, from *Escherichia coli*) were purchased from Sigma. Cholesterol (extra pure) was supplied by Merck (Darmstadt, Germany) and recrystallized twice from ethanol. Peptide markers for SDS−PAGE were purchased from Fluka. All other reagents were of analytical grade. Buffers were prepared in double glass-distilled water.

Peptide Synthesis and Purification. Peptides were synthesized by a solid-phase method on 4-methyl benzhydrylamine resin (0.05 mequiv) (*24*). The protecting group of tryptophan was removed by 20% piperidine in dry DMF. Labeling of the N-terminus of the peptides with rhodamine was done on the resin-bound peptide as previously described (*18*). The resin-bound peptides were cleaved from the resins by hydrogen fluoride (HF), and after HF evaporation and washing with dry ether, they were extracted with 50% acetonitrile/water. The peptides were further purified by RP-HPLC on a C_{18} reversed-phase Bio-Rad semipreparative column (250 × 10 mm, 300 Å pore size, 5 μm particle size). Prior to purification, the peptides were dissolved in 20% acetonitrile/water (5 mg/mL), and 200 μL was injected in each run. The column was eluted in 40 min, using a linear gradient of 10 to 60% acetonitrile in water, both containing 0.05% TFA (v/v), at a flow rate of 1.8 mL/min. Each crude peptide contained one major peak that was 50−70% pure by weight. The purified peptides were shown to be homogeneous (>98%) by analytical HPLC. The peptides were further subjected to amino acid analysis and electrospray mass spectroscopy to confirm their composition and molecular weight.

Preparation of Small (SUV) and Large (LUV) Unilamellar Vesicles. SUVs were prepared by sonication of PC/cholesterol (10:1 w/w) or PE/PG (7:3 w/w) dispersions as previously described (*25*). LUVs were prepared by extrusion from the same lipids as described in details previously (*26*). Vesicles were visualized using a JEOL JEM 100B electron microscope (Japan Electron Optics Laboratory Co., Tokyo, Japan) as follows. A drop of vesicles was deposited on a carbon-coated grid and negatively stained with uranyl acetate. Examination of the grids demonstrated that the vesicles were unilamellar with an average diameter of 20−50 nm in the case of SUV and 50−180 nm in the case of LUV.

Antibacterial Activity of the Peptides. The antibacterial activity of the peptides was examined in sterile 96-well plates (Nunc F96 microtiter plates) in a final volume of 100 μL as follows. Aliquots (50 μL) of a suspension containing bacteria at a concentration of 10^6 colony-forming units (CFU)/mL in culture medium (LB medium) were added to 50 μL of water containing the peptide in serial 2-fold dilutions in water (prepared from a stock solution of 1 mg/mL peptide in water). Inhibition of growth was determined by measuring the absorbance at 492 nm with a Microplate autoreader El309 (Bio-tek Instruments), after an incubation of 18−20 h at 37 °C. Antibacterial activities were expressed as the minimal inhibitory concentration (MIC), the concentration at which 100% inhibition of growth was observed after 18−20 h of incubation. The bacteria used were *E. coli* D-21, *Pseudomonas aeruginosa* ATCC 27853, *Acinetobacter baumini* ATCC 19606, *Bacillus megaterium* ATCC 6051, *Staphylococcus aureus* ATCC 25923.

Hemolysis of Human Red Blood Cells (hRBC). Fresh hRBC with EDTA were rinsed 3 times with PBS (35 mM

[1] Abbreviations: ATR-FTIR, attenuated total reflectance Fourier transform infrared; BHA, 4-methyl benzhydrylamine resin; Boc, butyloxycarbonyl; CD, circular dichroism; CFU, colony-forming units; HF, hydrogen fluoride; hRBC, human red blood cells; MIC, minimal inhibitory concentration; PBS, phosphate-buffered saline; PC, egg phosphatidylcholine; PE, *E. coli* phosphatidylethanolamine; PG, egg phosphatidylglycerol; Rho, carboxytetramethylrhodamine succinimidyl ester; RP-HPLC, reversed-phase high-performance liquid chromatography; SDS, sodium dodecyl sulfate; TFA, trifluoroacetic acid; TFE, 2,2,2-trifluoroethanol.

phosphate buffer/0.15 M NaCl, pH 7.3) by centrifugation for 10 min at 800 g and resuspended in PBS. Peptides dissolved in PBS were then added to 50 μL of a solution of the stock hRBC in PBS to reach a final volume of 100 μL (final erythrocyte concentration, 4% v/v). The resulting suspension was incubated under agitation for 60 min at 37 °C. The samples were then centrifuged at 800 g for 10 min. Release of hemoglobin was monitored by measuring the absorbance of the supernatant at 540 nm. Controls for zero hemolysis (blank) and 100% hemolysis consisted of hRBC suspended in PBS and Triton 1%, respectively.

CD Spectroscopy. The CD spectra of the peptides were measured with a Jasco J-500A spectropolarimeter after calibrating the instrument with (+)-10-camphorsulfonic acid. The spectra were scanned at 25 °C in a capped, quartz optical cell with a 0.5 mm path length. Spectra were obtained at wavelengths of 250 to 190 nm. Eight scans were taken for each peptide at a scan rate of 20 nm/min. The peptides were scanned at concentrations of $1.5 \times 10^{-5}-2.0 \times 10^{-4}$ M in PBS (35 mM phosphate buffer/0.15 M NaCl, pH 7.3) and in the presence of 1% SDS micelles. Due to a large light scattering effect, CD spectroscopy was not done in vesicles. Fractional helicities (*27*, *28*) were calculated as follows:

$$\frac{[\theta]_{222} - [\theta]^0_{222}}{[\theta]^{100}_{222} - [\theta]^0_{222}}$$

where $[\theta]_{222}$ is the experimentally observed mean residue ellipticity at 222 nm, and the values for $[\theta]^0_{222}$ and $[\theta]^{100}_{222}$, which correspond to 0 and 100% helix content at 222 nm, are estimated to be 2000 and 32 000 deg cm^2/dmol, respectively (*28*).

Oligomerization of the Peptides in Solution and Phospholipid Membrane Determined by Rhodamine Fluorescence Dequenching Measurements. Rhodamine-labeled peptide at different concentrations was added to 2 mL of PBS, and rhodamine fluorescence emission was tracked. Proteinase K (10 μg/mL) was then added, resulting in an increase in the fluorescence emission as a result of the dequenching of the rhodamine fluorescence. More proteinase K was added until no further increase in the fluorescence emission was observed. Excitation was set at 530 nm (8 nm slit) and emission was set at 582 nm (4 nm slit). All fluorescence measurements were performed at room temperature on a SLM-Aminco, Series 2 Spectrofluorimeter.

Determining the Oligomeric States of the Peptides by SDS−PAGE. The experiments were performed as described in ref *29*, except for a change in the sample preparation: HPLC-purified peptide and SDS (1:1 w/w) were dissolved in $CHCl_3$:MeOH (2:1 v/v). The solvents were evaporated under a stream of nitrogen, and then lyophilized. Subsequently, the peptides and SDS mixtures were resuspended in buffer composed of 0.065 M Tris-HCl, pH 6.8, and 10% glycerol by sonication. Fixing, staining, and destaining times were 1 min, 1 h, and overnight, respectively, to decrease diffusion effects.

Localization of the Environment of Tryptophan. The fluorescence emission spectrum of tryptophan was monitored in PBS, and in the presence of vesicles composed of either PE/PG (7:3, w/w) or PC/cholesterol (10:1. w/w). A 1-cm path length quartz cuvette that contained a final reaction volume of 2 mL was used in all experiments. Studies were performed on a SLM-Aminco, Series 2 Spectrofluorimeter, with excitation set at 280 nm, using a 4 nm slit, and emission set at 340 nm, using a 4 nm slit. In these fluorometric studies, SUVs were used to minimize differential light-scattering effects (*30*), and the lipid/peptide molar ratio was maintained high (>1000:1) so that the spectral contributions of free peptide would be negligible.

Binding of Peptides to Vesicles. The degree of peptide association with zwitterionic [PC/cholesterol (10:1 w/w)] or net negatively charged phospholipids [PE/PG (7:3 w/w)] was measured by adding increasing amounts of SUV to 0.5 μM peptide dissolved in PBS. The fluorescence intensity was measured in the time dependent mode, with excitation set at 467 nm, emission at 530 nm, and slits set to 8 nm, until a maximal intensity was achieved. Measurements were taken at several vesicle concentrations. The fluorescence values, f, were corrected by subtracting the corresponding blank (buffer with the same amount of vesicles). The increases in the fluorescence intensity, $[f - f_0]$, where f_0 is fluorescence intensity in the absence of vesicles, were plotted as a function of the lipid/peptide molar ratio.

The partition coefficient was determined by nonlinear least-squares (NLLSQ) fitting using the following equations:

$$f = f_{\text{bound}} f_{\max} + (1 - f_{\text{bound}}) f_0$$

$$f_{\text{bound}} = K_p L/(W + K_p L)$$

where f_{bound} is the fluorescence of bound peptide, $f_{\max}$ the fluorescence of full binding, K_p the partition coefficient, L molar lipid concentration, and W is the water concentration (55.56 M). NLLSQ analyses and data simulations were performed with the commercial software package: Origin 6.1 (MicroCal, Inc., Northampton, MA).

ATR-FTIR Measurements. Spectra were obtained with a Bruker equinox 55 FTIR spectrometer equipped with a deuterated triglyceride sulfate (DTGS) detector and coupled with an ATR device as previously described (*31*). Previous to sample preparations, the trifluoroacetate (CF_3COO^-) counterions which strongly associate to the peptide were replaced with chloride ions through several lyophilizations of the peptides in 0.1 M HCl to eliminate absorption band near 1673 cm^{-1} (*32*). Lipid−peptide mixtures were prepared by dissolving them together in a 1:2 MeOH/CH_2Cl_2 mixture and drying under a stream of dry nitrogen while moving a Teflon bar back and forth along the ZnSe prism. Polarized spectra were recorded and the respective pure phospholipids in each polarization were subtracted to yield the difference spectra. The background for each spectrum was a clean ZnSe prism. Hydration of the sample was achieved by introduction of excess of deuterium oxide (^2H_2O) into a chamber placed on top the ZnSe prism in the ATR casting, and incubation for 2 h prior to acquisition of spectra. H/D exchange was considered complete due to the complete shift of the amide II band. Any contribution of ^2H_2O vapor to the absorbance spectra near the amide I′ peak region was eliminated by subtraction of the spectra of pure lipids equilibrated with ^2H_2O under the same conditions.

ATR-FTIR Data Analysis. Prior to curve fitting, a straight baseline passing through the ordinates at 1700 and 1600 cm^{-1} was subtracted. To resolve overlapping bands, the spectra

were processed using PEAKFIT (Jandel Scientific, San Rafael, CA) software. Second-derivative spectra accompanied by 13-data-point Savitsky-Golay smoothing were calculated to identify the positions of the components bands in the spectra. These wavenumbers were used as initial parameters for curve fitting with Gaussian component peaks. Position, bandwidths, and amplitudes of the peaks were varied until (i) the resulting bands shifted by no more than 2 cm^{-1} from the initial parameters, (ii) all the peaks had reasonable half-widths ($<20-25$ cm^{-1}), and (iii) good agreement between the calculated sum of all components and the experimental spectra were achieved ($r^2 > 0.99$). The relative contents of different secondary structure elements were estimated by dividing the areas of individual peaks, assigned to particular secondary structure, by the whole area of the resulting amide I′ band. The results of four independent experiments were averaged.

Analysis of the Polarized ATR-FTIR Spectra. The ATR electric fields of incident light were calculated as follows (*33*, *34*).

$$E_x = \frac{2\cos\theta\sqrt{\sin^2\theta - n_{21}^2}}{\sqrt{(1-n_{21}^2)[(1+n_{21}^2)\sin^2\theta - n_{21}^2]}}$$

$$E_y = \frac{2\cos\theta}{\sqrt{1-n_{21}^2}}$$

$$E_z = \frac{2\sin\theta\cos\theta}{\sqrt{(1-n_{21}^2)[(1+n_{21}^2)\sin^2\theta - n_{21}^2]}}$$

where θ is the angle of a light beam to the prism normal at the point of reflection (45°), and $n_{21} = n_2/n_1$ [n_1 and n_2 are the refractive indices of ZnSe (taken as 2.4) and the membrane sample (taken as 1.5), respectively]. Under these conditions, E_x, E_y, and E_z are 1.09, 1.81, and 2.32, respectively. The electric field components together with the dichroic ratio [defined as the ratio between absorption of parallel to the plane of the reflections in the ZnSe crystal (*35*), A_p, and perpendicularly polarized incident light, A_s] are used to calculate the orientation order parameter, *f*, by the following formula:

$$f = \frac{2(E_x^2 - R^{ATR}E_y^2 + E_z^2)}{h(3\cos^2\alpha - 1)(E_x^2 - R^{ATR}E_y^2 - 2E_z^2)}$$

Lipid order parameters were obtained from the symmetric (~2853 cm^{-1}) and antisymmetric (~2922 cm^{-1}) lipid stretching mode setting $\alpha = 90°$ (*34*).

Increasing Membrane Permeability Induced by the Peptides. Membrane destabilization, which results in the collapse of a diffusion potential, was detected fluorimetrically as previously described using the voltage sensitive dye diS-C_2-5 (*36*, *37*). Fluorescence was monitored using excitation and emission wavelengths at 620 and 670 nm, respectively. The percentage of fluorescence recovery, F_t, was defined by

$$F_t = [(I_t - I_o)/(I_f - I_o)]100\%$$

where I_t is the fluorescence observed after addition of a peptide at time *t*; I_o is the fluorescence after addition of valinomycin; and I_f is the total fluorescence prior to the addition of valinomycin.

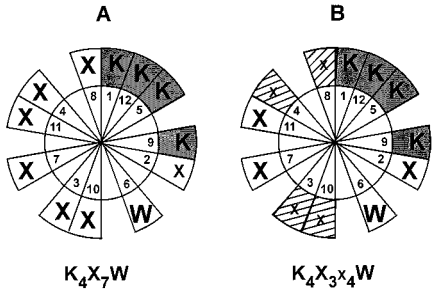

FIGURE 1: Schiffer Edmundson wheel projection (*40*) of the all-L-amino acids peptides (A), and their diastereomers (B). Dark background indicates hydrophilic amino acids (Lys). Empty background indicates hydrophobic amino acids and dashed background indicates hydrophobic D-amino acids. **X** represents one of the aliphatic amino acids Gly, Ala, Val, Ile, and Leu and **x** represents one of the aliphatic D-amino acids Ala, Val, Ile, and Leu.

Tryptophan Quenching Experiments. Brominated phospholipids (Br-PC) used as quenchers of tryptophan fluorescence are suitable for probing the membrane insertion of peptides, since they act over a short distance and do not drastically perturb the membrane (*38*, *39*). The diastereomers, each of which contains one tryptophan residue, were added (final concentration of 0.5 μM) to 2 mL of buffer PBS containing 43.4 μL (500 μM) of Br−PC/PE/PG (2.5/4.5/3 w/w) or Br-PC/PC (2.5/7.5 w/w) SUV, thus establishing a lipid /peptide ratio of 1000:1. After the emitted fluorescence was stabilized (10−60 min incubation at room temperature), an emission spectrum of the tryptophan was recorded using a SLM-Aminco, Series 2 Spectrofluorometer, with excitation set at 280 nm (4 nm slit). SUV composed of Br-PC/PE/PG (2.5/4.5/3 w/w) or Br-PC/PC (2.5/7.5 w/w), which contained either 6,7 Br-PC or 9,10 Br-PC, were used. Three separate experiments were conducted for each peptide. In control experiments, PC/PE/PG (2.5/4.5/3 w/w) or PC SUV without Br-PC were used.

Examination of Bacterial Membrane and Large Unilamellar Vesicles (LUVs) Damage by Electron Microscopy. Samples containing *E. coli* ATCC 25922 (1×10^6 CFU/mL) in LB medium were incubated with the peptides at their MIC and 60% of the MIC for 1 h and then centrifuged for 10 min at 300*g*. The pellets were resuspended, and a drop containing the bacteria was deposited onto a carbon-coated grid and negatively stained with phosphotungstic acid (PTA), 2% pH 6.8. The grids were examined using a JEOL JEM 100B electron microscope (Japan Electron Optics Laboratory Co., Tokyo, Japan). The effect of the peptides on PE/PG (7:3 w/w) LUV was examined similarly by incubating the peptides for 30 min at a peptide to lipid molar ratios at which the peptides exhibited 50% of their maximal activity in the membrane permeability study.

RESULTS

Peptides Design. Five different all L-amino acid model peptides and their diastereomers were synthesized. Their sequence $KX_3KWX_2KX_2K$ (X = Gly, Ala, Val, Ile, or Leu) was designed to create a perfect amphipathic α-helical structure, as revealed by Schiffer and Edmundson wheel projection (*40*) (Figure 1A). In each diastereomer, besides

Table 1: Sequences, Designations, Net Charge, Hydrophobicity, and Molecular Weight of the Peptides Investigated

Peptide Designation	Sequence[a,b]	Net charge	Hydrophobicity (% of AcN)[c]	Molecular Weight
K_4G_7W	K G G G K W G G K G G K – NH_2	+5	17.1	1115
K_4A_7W	K A A A K W A A K A A K – NH_2	+5	20.0	1213
K_4V_7W	K V V V K W V V K V V K – NH_2	+5	25.8	1409
K_4I_7W	K I I I K W I I K I I K – NH_2	+5	36.8	1508
K_4L_7W	K L L L K W L L K L L K – NH_2	+5	43.0	1508
$K_4A_3a_4W$	K A **A** **A** K W A **A** K **A** A K – NH_2	+5	21.4	1213
$K_4V_3v_4W$	K V **V** **V** K W V **V** K **V** V K – NH_2	+5	26.6	1409
$K_4I_3i_4W$	K I **I** **I** K W I **I** K **I** I K – NH_2	+5	34.0	1508
$K_4L_3l_4W$	K L **L** **L** K W L **L** K **L** L K – NH_2	+5	38.4	1508

[a] Bold and underlined letters are D-amino acids. [b] The C-terminus is amidated [c] The percentage of acetonitrile (AcN) that elute the peptides using C18 RP-HPLC at a linear gradient of AcN/water containing 0.05% TFA.

Table 2: Minimal Inhibitory Concentration (μM) of the Peptides

	minimal inhibitory concentration (μM)[a]				
peptide designation	*E. coli* (D21)	*A. calcoaceticus* (AC11)	*P. aeruginosa* (ATCC 27853)	*B. subtilis* (ATCC 6051)	*S. aureus* (ATCC 25922)
K_4G_7W	200	200	200	200	200
K_4A_7W	200	200	200	200	200
K_4V_7W	70	100	100	2.8	150
K_4I_7W	150	>200	>200	30	200
K_4L_7W	12.5	3	>200	1.25	18.1
$K_4A_3a_4W$	>200	>200	>200	>200	>200
$K_4V_3v_4W$	150	200	>200	60	>200
$K_4I_3i_4W$	19.3	100	>200	3.5	>200
$K_4L_3l_4W$	15	15	7.5	1.25	30
Cecropin B	2.3	1.5	3	0.75	2.4
Tetracycline	3	3	50	6	0.75

[a] Results are the mean of three independent experiments each performed in duplicates, with standard deviation not exceeding 20%.

the one containing Gly, four hydrophobic L-amino acids were substituted for their corresponding D-amino acids and one Trp to serve as an intrinsic fluorescent probe (Figure 1B). Table 1 presents the sequence of the peptides, their designations, net charge, hydrophobicity (presented as the percentage of acetonitrile required to elute the peptide by using RP-HPLC) and molecular weight.

Antibacterial and Hemolytic Activity of the Peptides. We tested the potential of the peptides to inhibit the growth of different species of bacteria and the extent of their hemolytic activity against the highly susceptible human erythrocytes. The antibiotic tetracycline and cecropin, a native antimicrobial peptide (*41*), served as controls. The set of test bacteria included three Gram negative species (*E. coli*, *A. baumannii*, and *P. aeruginosa*) and two Gram positive species (*B. subtilis* and *S. aureus*). Table 2 presents the MIC of the peptides and Figure 2 the dose response of their hemolytic activity. A MIC less than 50 μM is considered as a significant activity.

Consistently, peptides containing the most hydrophobic amino acids (L, I, V) are highly hemolytic whereas their diastereomers are substantially less hemolytic. Among the all L-amino acid peptides, only K_4L_7W was active on most bacteria tested. K_4V_7W and K_4I_7W were selectively active only on *B. subtillis*, known as a very sensitive bacterium. Interestingly, among the diastereomers, only $K_4L_3l_4W$ was active on all bacteria tested and $K_4I_3i_4W$ increased its spectrum of activity.

Aggregation of the Peptides in Aqueous Solution Examined by Circular Dichroism Spectroscopy. Circular dichroism spectroscopy was used to examine the secondary structure of the all L-amino acid peptides in aqueous solution (PBS) at different concentrations (1.5×10^{-5}M-2×10^{-4}M). K_4G_7W and K_4A_7W have a random structure with a characteristic minimum near 200 nm. The CD spectra of K_4V_7W (1.5×10^{-5}M) revealed that the peptide is predominantly random coil. However, as the concentration is increased (up to 2×10^{-4}M), a band near 214 nm appears, indicating the presence of a β-sheet structure. At all concentrations examined, K_4L_7W adopts ~45% α-helical structure, as calculated from its minimum at 222 nm, while K_4I_7W adopts predominantly β-sheet structure as deduced from the band near 214 nm. An amphipatic peptide can form a distinct secondary structure in solution only if it oligomerizes such that the hydrophobic surfaces are packed one against another and the hydrophilic surfaces face the solution. Together with the rhodamine quenching experiments described below we can conclude that K_4V_7W, K_4I_7W, and K_4L_7W oligomerize in solution. CD experiments with the diastereomers did not give significant signals. Circular dichroism in proteins is a phenomenon that results when chromophores (mainly nonbonding electrons of the carbonyl

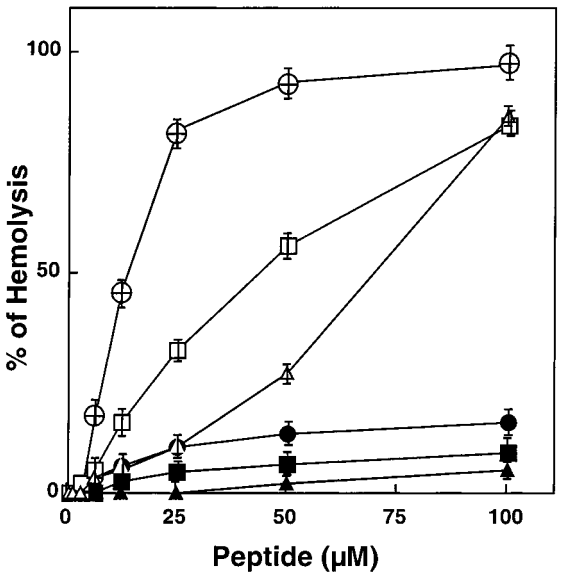

FIGURE 2: Dose-response of the hemolytic activity of the peptides toward hRBC. The assay was performed as described in the Materials and Methods. Designations are as follows: K_4V_7W (△); $K_4V_3v_4W$ (▲); K_4I_7W (□); $K_4I_3i_4W$ (■); K_4L_7W (⊕); $K_4L_3l_4W$ (●). K_4G_7W, K_4A_7W, and $K_4A_3a_4W$ had no hemolytic activity and therefore are not shown. The results are the mean of three separate experiments.

oxygens) in an asymmetrical environment interact with polarized light. A diastereomer, as opposed to all-L- or all-D-amino acid peptides, is composed of both D- and L-amino acid that have opposite magnetic dipole moment and optical activity. The opposite circularly polarized absorption components of the D- and L-amino acid can cancel out and decrease the overall absorbance of the right-handed helix.

Oligomeric State of the Diastereomeric Peptides in Aqueous Solution and Phospholipid Membranes. The ability of the diastereomeric peptides to self-associate in aqueous solution and net negatively charged PE/PG (7:3, w/w) phospholipid membranes was investigated using Rho-labeled peptides (*42*). When rhodamine-labeled monomers are associated and the rhodamine probes are in close proximity, the result is self-quenching of the emission fluorescence. The fluorescence of rhodamine is only slightly sensitive to the polarity of its environment and therefore can be studied in aqueous solution and lipids (*43*). A difference in the fluorescence intensity between a peptide treated with proteolytic enzyme and a nontreated peptide indicates whether a peptide is self-associated or not. The fluorescence of the rhodamine-labeled peptides Rho-K_4G_7W, Rho-$K_4A_3a_4W$, Rho-$K_4V_3v_4W$, Rho-$K_4I_3i_4W$, and Rho-$K_4L_3l_4W$ in PBS at different concentrations (0.1, 0.5, 1, and 2 μM) reached the same level before, or after their enzymatic degradation (data not shown). These results indicate that the peptides do not aggregate in aqueous solution. A similar level of fluorescence was observed upon the addition of PE/PG vesicles (data not shown), indicating that the peptides remain as monomers upon their binding to the membrane. In contrast, the fluorescence of the rhodamine-labeled peptides Rho-K_4V_7W, Rho-K_4I_7W, and Rho-K_4L_7W was highly quenched in solution but increased 5−15-fold after enzymatic degradation (data not shown). Furthermore, the observed fluorescence upon addition of PE/PG vesicles was less than after enzymatic degradation (data not shown), indicating that the peptides remain as oligomers (at least partially) upon binding to the membrane.

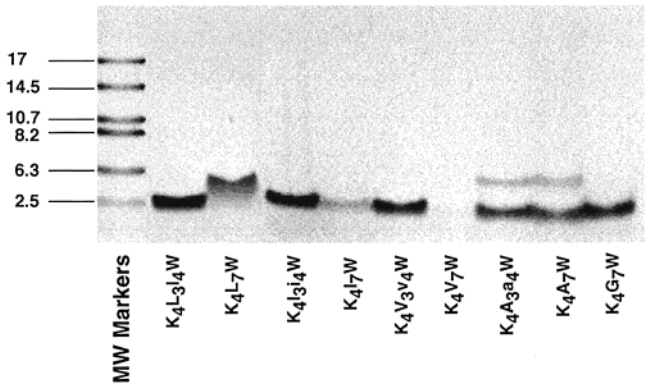

FIGURE 3: Determining the aggregation states of the peptides by Tricine SDS−PAGE. Samples were prepared as described in the Materials and Methods. The molecular weight of the peptides is as follows: K_4G_7W, 1115; K_4A_7W and $K_4A_3a_4W$, 1213; K_4V_7W and $K_4V_3v_4W$, 1405; K_4I_7W and $K_4I_3i_4W$, 1508; K_4L_7W and $K_4L_3l_4W$, 1508.

Oligomerization of the Peptides in SDS−PAGE. The aggregation state of several membrane proteins was determined using SDS, a membrane-mimetic environment (*44*, *45*). Here, SDS−PAGE (Figure 3) revealed substantial differences between most of the all-L-amino acid peptides and their diastereomeric analogues. The major bands of K_4V_7W and K_4I_7W were located at the interface between the stacking and the separating gels, indicating the existence of large aggregates that were not able to enter into the separating gel. However, a small fraction of K_4I_7W was observed in a band corresponding to a monomer. Furthermore, the dominant form of K_4L_7W was an oligomer, presumably a dimer. In contrast, the diastereomeric analogues containing Leu, Ile, and Val were monomers, whereas that of Ala displayed also only a small fraction of a dimer. It should be noted that the bands of the monomeric peptides are located at higher molecular weights than expected. This may result from the hydrophobic character of the peptides as compared to the hydrophilic character of the molecular weight markers.

Localization of the Environment of the Tryptophan. The interaction of the peptides with vesicles consisting of PC/cholesterol 10:1 w/w [a phospholipid composition used for mimicking the major components of the outer leaflet of human erythrocytes (*46*)] or PE/PG 7:3 w/w [a phospholipid composition typical of *E. coli* (*47*)] was monitored using the fluorescence emission spectrum of the tryptophan. Table 3 summarizes the results. All the peptides, except K_4I_7W, had emission maxima of 351 nm in solution. When PE/PG vesicles were added to the aqueous solutions containing the peptides, blue shifts in the emission maxima were observed for most of the peptides. The change in the spectrum of tryptophan reflects its relocation to a more hydrophobic environment. Under our experimental conditions, no blue shifts in the emission maxima of K_4G_7W or $K_4A_3a_4W$ were observed. However, a blue shift toward 343 ± 2 nm was observed with the all L-amino acid K_4A_7W. Indeed, K_4A_7W but not its diastereomer slightly increased membrane permeability. The absence of a blue shift suggests that these two peptides either bind very weakly to the vesicles or, upon binding, are not immersed into the hydrophobic environment

Table 3: Tryptophan Emission Maxima of the Peptides in Solution, in the Presence of PE/PG (7:3, w/w) or PC/Cholesterol (10:1, w/w) Vesicles

peptide designation	PBS	PE/PG[a]	PC/chlesterol[a]
K_4G_7W	351 ± 1	351 ± 1	351 ± 1
K_4A_7W	351 ± 1	343 ± 2	351 ± 1
K_4V_7W	351 ± 1	335 ± 1	343 ± 1
K_4I_7W	ND[b]	ND	ND
K_4L_7W	351 ± 1	336 ± 1	338 ± 1
$K_4A_3a_4W$	351 ± 1	351 ± 1	351 ± 1
$K_4V_3v_4W$	351 ± 1	337 ± 1	351 ± 1
$K_4I_3i_4W$	351 ± 1	336 ± 1	351 ± 1
$K_4L_3l_4W$	351 ± 1	337 ± 1	351 ± 1

[a] A lipid to peptide molar ratio of 1000:1 was used in all cases. [b] ND, not determined.

of the lipids. The second option is more reasonable in light of previous studies showing that all lysine containing peptides bind to negatively charged vesicles (*48*) (see next paragraph). In the presence of PC/cholesterol vesicles, only the all L-peptides K_4V_7W and K_4L_7W exhibited blue shifts in their emission maxima.

Binding Studies. Peptides that exhibited blue shifts in their emission maxima were subjected to binding experiments using the intrinsic fluorescence of tryptophan as described in the Materials and Methods. The conventional binding curves are shown in Figure 4A for the diastereomers in PE/PG and in Figure 4B for the all L-peptides K_4V_7W and K_4L_7W in PE/PG (crossed symbols) and PC/cholesterol vesicles (empty symbols). The surface partition coefficients were determined only for the diastereomeric peptides (which do not oligomerize in solution) by nonlinear least-squares (NLLSQ) fitting and were found to be 1.9 (±0.3) × 10^6 M^{-1}, 1.1 (±0.2) × 10^6 M^{-1} and 2.0 (±0.3) × 10^5 M^{-1}, for $K_4L_3l_4W$, $K_4I_3i_4W$, and $K_4V_3v_4W$, respectively. These numbers are the mean of three independent experiments, and correspond to free energy (ΔG) values of −8.6 ± 0.1, −8.2 ± 0.1, and −7.2 ± 0.1 kcal/mol for the three peptides, respectively. Interestingly, the trend of estimated ΔG values for these peptides based on studies done with lysine-containing peptides (*48*) and the contribution of the aliphatic amino acids (*49*) agree with our measurements. The estimated ΔG values are ∼−9.5, −8.0, and −5.7 kcal/mol for the Leu, Ile, and Val containing peptides, respectively. On the basis of studies by Murray and White, we would also expect ΔG values of ∼−4.7 and −5.7 kcal/mol for the Ala- and the Gly-containing peptides. However, the inability to detect a blue shift in the tryptophan signals indicate that the tryptophans are not buried in close proximity to the lipids, in agreement with their inability to lyse erythrocytes or to kill bacteria. To ascertain that the Ala- and Gly-containing peptides do indeed bind to the surface of the membrane, we used fluorescence resonance energy transfer from the peptides' tryptophan to dansyl chromophores attached to the headgroup of lipid vesicles. When the peptides were added to vesicles containing 1% dansyl-phosphatidylethanolamine (DNS-PE), the dansyl fluorescence substantially increased, indicating that they bind to the membrane (data not shown).

The binding curves of the all L-amino acid peptides K_4L_7W and K_4V_7W with PE/PG and PC/cholesterol show that saturation occurred at lipid:peptide molar ratios close to those observed with the diastereomers, suggesting that they have

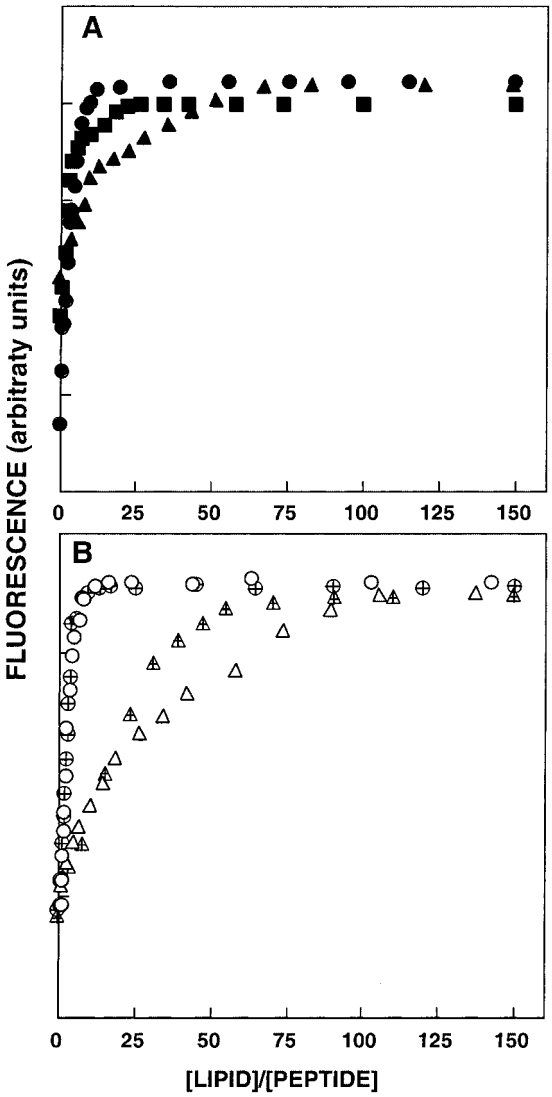

FIGURE 4: Increases in the fluorescence of the diastereomeric peptides upon titration with PE/PG vesicles (A), and all L-amino acid peptides with PE/PG and PC/cholesterol (B), with excitation wavelength set at 280 nm and emission at 340 nm. The experiment was performed at 25 °C in PBS (peptide concentration 0.5 μM). Designation: $K_4V_3v_4W$ (▲); $K_4I_3i_4W$ (■); $K_4L_3l_4W$ (●); K_4V_7W with PE/PG (cross-hatched triangle); K_4L_7W with PE/PG (⊕); K_4V_7W with PC/cholesterol (△); K_4L_7W with PC/cholesterol (○).

similar partition coefficients. Furthermore, the binding curves of these two peptides with PE/PG or PC/cholesterol are similar, indicating that the affinity of the all L-amino acid peptide to membranes results predominantly from hydrophobic interactions rather than electrostatic attractions.

Secondary Structure of the Diastereomers in PE/PG Phospholipid Membranes as Determined by FTIR Spectroscopy. FTIR spectroscopy was used to determine the secondary structure of the peptides when bound to phospholipid membranes. Helical and unordered structures can contribute to the amide I vibration at almost identical wavenumbers, and it is difficult to determine the precise proportion of helix and random coil structures from the IR spectra. However, the exchange of hydrogen with deuterium makes it possible, sometimes, to differentiate α-helical components from a random structure, since the absorption of the random structure shifts to a greater extent than the α-helical component after deuteration (*50*). Therefore, we examined

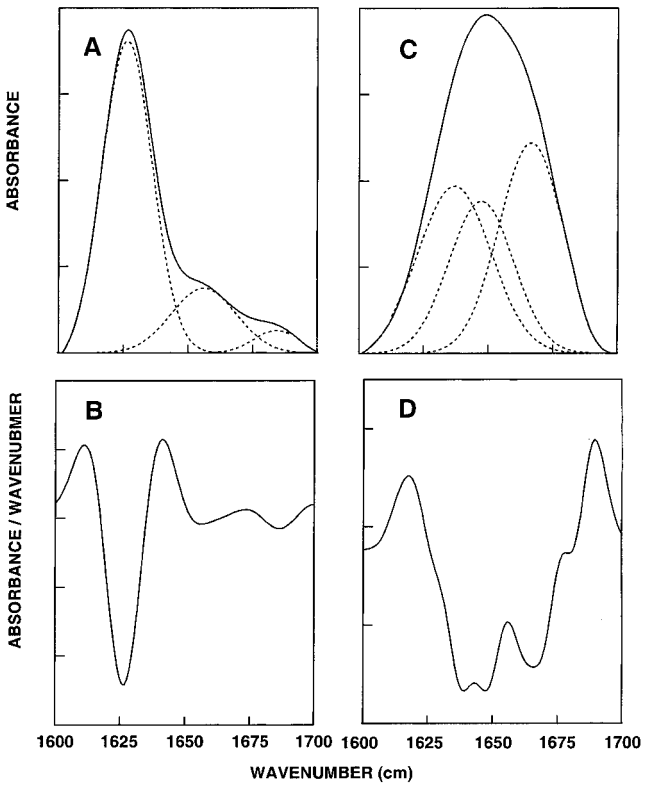

FIGURE 5: FTIR spectra deconvolution of the fully deuterated amide I′ band (1600−1700 cm^{-1}) of K_4I_7W (panel A) and $K_4I_3i_4W$ (panel C) in PE/PG (7:3, w/w) multibilayers. The second derivatives, calculated to identify the positions of the components bands in the spectra, are shown in panel B for K_4I_7W and in panel D for $K_4I_3i_4W$. The component peaks are the result of curve-fitting using a Gaussian line shape. The sums of the fitted components superimpose on the experimental amide I′ region spectra. Continuous lines represent the experimental FTIR spectra after Savitzky-Golay smoothing; the broken lines represent the fitted components. A 60:1 lipid/peptide molar ratio was used.

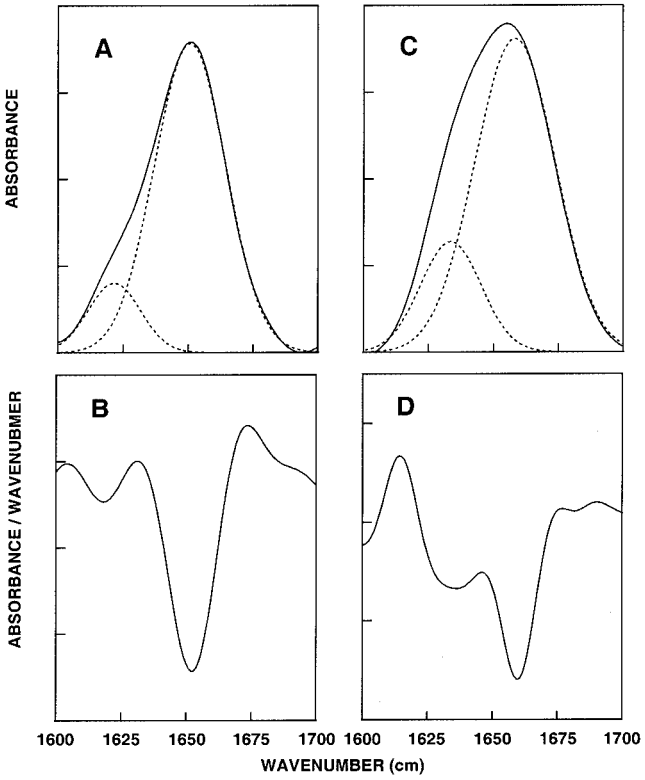

FIGURE 6: FTIR spectra deconvolution of the fully deuterated amide I′ band (1600−1700 cm^{-1}) of K_4L_7W (A) and $K_4L_3l_4W$ (C) in PE/PG (7:3, w/w) multibilayers. The second derivatives, calculated to identify the positions of the components bands in the spectra, are shown in panel B for K_4L_7W and in panel D for $K_4L_3l_4W$. Details are as depicted in the legend to Figure 5. A 60:1 lipid/peptide molar ratio was used.

the IR spectra of the peptides after complete deuteration (see Materials and Methods). K_4G_7W bound on the surface of PE/PG, did not bind to PC/cholesterol membrane, and was inactive in all functional assays. None of the diastereomers do bind, or only weakly bind, to PC/cholesterol membranes (no blue shift) and were therefore not examined. Examples of the amide I′ (deuterated amide) region spectra of K_4I_7W and $K_4I_3i_4W$ bound to PE/PG (7:3 w/w) multibilayers are shown in Figure 5, panels A and C, respectively, and those for K_4L_7W and $K_4L_3l_4W$ in Figure 6, panels A and C, respectively. Second derivatives accompanied by 13-data-point Savitsky-Golay smoothing were calculated to identify the positions of the component bands in the spectra (panels B and D in Figures 5 and 6). These wavenumbers were used as initial parameters for curve fitting with Gaussian component peaks. Table 4 summarizes the assignments, wavenumbers (ν), and relative areas of the component peaks.

The assignment of the different secondary structures to the various amide I′ regions was calculated according to the values taken from Jackson and Mantsch (*51*) (Table 4). The amide I′ region of an α-helical structure is located between 1650 and 1655 cm^{-1}, and the amide I′ region from 1656 to 1670 cm^{-1} is characteristic of a 3_{10}-helix or a distorted helix (*52*). For example, the major amide I′ band of K_4L_7W is located at ∼1651 cm^{-1} (Figure 6A), characteristic of an α-helical structure, whereas that of $K_4L_3l_4W$ is located at ∼1658 cm^{-1} (Figure 6C), suggesting a distorted or 3_{10}-helix. Due to the amphipathic design of the peptides (Figure 1), we expect formation of a helical structure (a classical α-helix or a distorted one) in order to orient the hydrophobic face toward the lipidic part of the membrane. Changes in the stability of an α-helical structure bound on the surface of membranes have been previously observed by others (*22*, *53*, *54*). The assignment of a ∼1657 cm^{-1} component to a distorted helix was reported for a transmembrane domain in bacteriorhodopsin and other proteins (*55*, *56*), although it is not known if the assignment will hold for transmembrane helices. These studies demonstrated that distorted α-helical structures are characterized by increased amide I′ frequencies. The secondary structures of K_4I_7W and K_4L_7W (the only peptides that were highly hemolytic) were also determined in PC/cholesterol. In these membranes, both peptides had a high percentage of α-helical structure. The major amide I′ band of K_4I_7W is located at ∼1651 cm^{-1} (70 ± 5%) and the second at 1623 ±2 (30 ± 5%). Similarly, the major amide I′ band of K_4L_7W is located at ∼1652 cm^{-1} (85 ± 5%) and the second at 1624 ± 1 (15 ± 5%). It should be noted that absorption of a normal α-helix in short peptides has been assigned also to higher wavelengths, typically 1660 cm^{-1} for 12 residues peptides (the same length of the peptides in the present study) (*57*).

Membrane Permeability Induced by the Diastereomeric Peptides. The peptides were mixed at various concentrations with vesicles that had been pretreated with valinomycin and the fluorescent dye diS-C_2-5. The kinetics of the fluorescence recovery was monitored with time. The maximum level

Table 4: Assignment, Wavenumbers (ν), and Relative Areas of the Component Peaks Determined from the Deconvolution of the Amide I′ Bands of the Peptides Incorporated into PE/PG (7:3 w/w) Multibilayers[a]

peptide designation	aggregated β-Sheet		β-sheet		random coil and α-helix		α-helix		distorted/3_{10}-helix	
	ν (cm^{-1})	area (%)	ν (cm^{-1})	area (%)	ν (cm^{-1})	area (%)	ν (cm^{-1})		ν (cm^{-1})	area (%)
K_4A_7W					1647 ± 2	100				
K_4V_7W	1622 ± 2	75 ± 2			1648 ± 2	25 ± 1				
K_4I_7W	1626 ± 1	73 ± 2							1656 ± 2	27 ± 3
K_4L_7W	1621 ± 2	15 ± 5					1651 ± 1	85 ± 5		
$K_4A_3a_4W$			1635 ± 1	20 ± 2	1646 ± 3	35 ± 3			1666 ± 1	45 ± 5
$K_4V_3v_4W$					1642 ± 2	60 ± 5			1666 ± 1	40 ± 5
$K_4I_3i_4W$			1637 ± 2	35 ± 3	1647 ± 2	30 ± 5			1666 ± 1	35 ± 5
$K_4L_3l_4W$			1634 ± 1	25 ± 5					1658 ± 1	75 ± 5

[a] A 1:60 peptide:lipid molar ratio was used. The results are the average of four independent experiments.

Table 5: TR Dichroic Analysis of Phospholipid Multibilayers

	peptide:lipid molar ratio	R of $\nu_{antisymmetric}(CH_2)$	f $\nu_{antisymmetric}(CH_2)$
PE/PG		1.35 (±0.02)	0.30 (±0.01)
PE/PG + $K_4I_3i_4W$	1:60	1.42 (±0.03)	0.27 (±0.01)
PE/PG + $K_4I_3i_4W$	1:50	1.43 (±0.01)	0.26 (±0.01)
PE/PG + $K_4I_3i_4W$	1:40	1.43 (±0.02)	0.26 (±0.01)
PE/PG + $K_4I_3i_4W$	1:30	1.48 (±0.02)	0.24 (±0.01)
PE/PG + $K_4I_3i_4W$	1:20	1.55 (±0.02)	0.20 (±0.01)
PE/PG + $K_4L_3l_4W$	1:60	1.41 (±0.03)	0.27 (±0.01)
PE/PG + $K_4L_3l_4W$	1:50	1.42 (±0.03)	0.27 (±0.01)
PE/PG + $K_4L_3l_4W$	1:40	1.42 (±0.02)	0.27 (±0.01)
PE/PG + $K_4L_3l_4W$	1:30	1.42 (±0.02)	0.27 (±0.01)
PE/PG + $K_4L_3l_4W$	1:20	1.42 (±0.02)	0.27 (±0.01)

reached as a function of peptide concentration was determined (shown for the all L-amino acid peptides in Figure 7, panels A and B for PE/PG and PC/cholesterol, respectively, and for the diastereomers in Figure 8, panels A and B, for PE/PG and PC/cholesterol, respectively). Importantly, the data reveal a marked decrease in the ability of the diastereomeric peptides to increase the permeability of PC/cholesterol compared to PE/PG.

Peptide Depth of Penetration in the Membrane as Determined by Tryptophan-Quenching Experiments. The PE/PG SUV contained bromolipids [1-palmitoyl-2-(dibromo-stearoyl) phosphatidylcholine] with bromines at the 6,7- and 9,10-positions (Br-PC) which served as a molecular ruler. Br is a quencher of tryptophan fluorescence with an r^6 dependence and an apparent R_0 of 9 Å (*38*). The peptide-to-lipid molar ratio in these experiments was kept low (1:1000) to eliminate the contribution of free peptide. The results revealed significant quenching (9−24%) for the all L-amino acid peptides and their diastereomers containing Val, Ile, and Leu only with 6,7-Br-PC, suggesting that these peptides do not penetrate deeply into the membrane, and instead lie close to the membrane interface (*58*, *59*) (graphs not shown).

Orientation of the Phospholipid Membrane and the Effect of Peptide Binding on the Acyl Chain Order. Polarized ATR-FTIR was used to determine the orientation of the lipid membrane. The symmetric [$\nu_{sym}(CH_2) \approx 2850$ cm^{-1}] and the antisymmetric [$\nu_{antisym}(CH_2) \approx 2920$ cm^{-1}] vibrations of lipid methylene C−H bonds are perpendicular to the molecular axis of a fully extended hydrocarbon chain. Thus, measuring the dichroism of infrared light absorbance can reveal the order and orientation of the membrane sample relative to the prism surface. Table 5 shows the calculated R values and their corresponding f values based on the stronger $\nu_{antisym}(CH_2)$. The R value for PE/PG indicates that the phospholipid membrane is well-ordered (*34*, *60*, *61*). The observed antisymmetric and symmetric peaks at 2921.9 ± 0.2 cm^{-1} and 2852.7 ± 0.3 cm^{-1}, respectively, indicate that the PE/PG membranes are predominantly in a liquid-crystalline phase similar to biological cell membranes (*34*, *62*).

The effect of the two most active diastereomers, $K_4L_3l_4W$ and $K_4I_3i_4W$, on the PE/PG multibilayer acyl-chain order was examined. Peptide-to-lipid molar ratios ranging from 1:60 to 1:20 were chosen according to binding studies (Figure 4), and the activity of the peptides observed in the membrane permeability study (Figures 7,8). Table 5 summarizes the R values and the corresponding order parameters, f, at the various peptide-to-lipid molar ratios. Interestingly, whereas the incorporation of $K_4L_3l_4W$ into the membrane did not significantly change the lipid order, a dose-dependent disruption effect was observed with $K_4I_3i_4W$. This difference occurs despite their similar ability to increase membrane permeability (Figures 7and 8) and depth of penetration (bromine quenching experiments), suggesting that they use different mechanisms to increase membrane permeability. Since both parental peptides K_4L_7W and K_4I_7W highly aggregate in solution and membranes, significant variations in the experimental results were observed preventing reliable conclusions from being drawn.

Effect of the Peptides on the Morphology of PE/PG LUVs Examined by Electron Microscopy. The peptides were added to PE/PG LUVs [membranes typical of *E. coli* (*47*)] at peptide-to-lipid molar ratios corresponding to a ∼50% increase in membrane permeability (Figures 7A, 8A): 1:20 with K_4I_7W, 1:20 with K_4L_7W, 1:10 with $K_4I_3i_4W$, and 1:25 with $K_4L_3l_4W$. After a short incubation time (30 min), a drop of a sample was removed, fixed, and examined using transmission electron microscopy. $K_4L_3l_4W$ caused micelli-

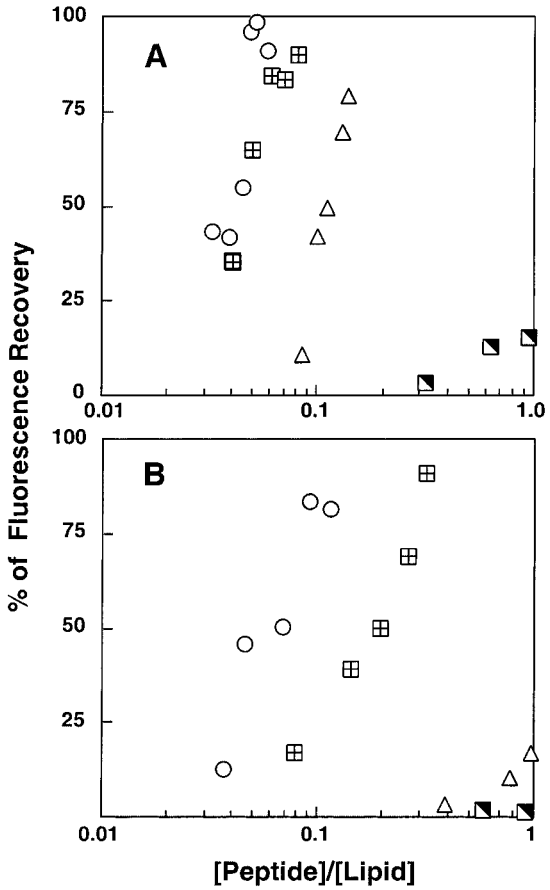

FIGURE 7: Maximal dissipation of the diffusion potential in PE/PG (A) and PC/cholesterol (B) vesicles induced by the all L-amino acid peptides. The peptides were added to isotonic K^+ free buffer containing SUV composed of PE/PG (7:3, w/w), preequilibrated with the fluorescent dye 3,3′-diethylthio-dicarbocyanine iodide and valinomycin. Fluorescence recovery was measured 10−20 min after the peptides were mixed with the vesicles. Designations are as follows: K_4A_7W (◥); K_4V_7W (△); K_4I_7W (⊞); K_4L_7W (○). Results are the mean of three independent experiments with standard deviation not exceeding 5%.

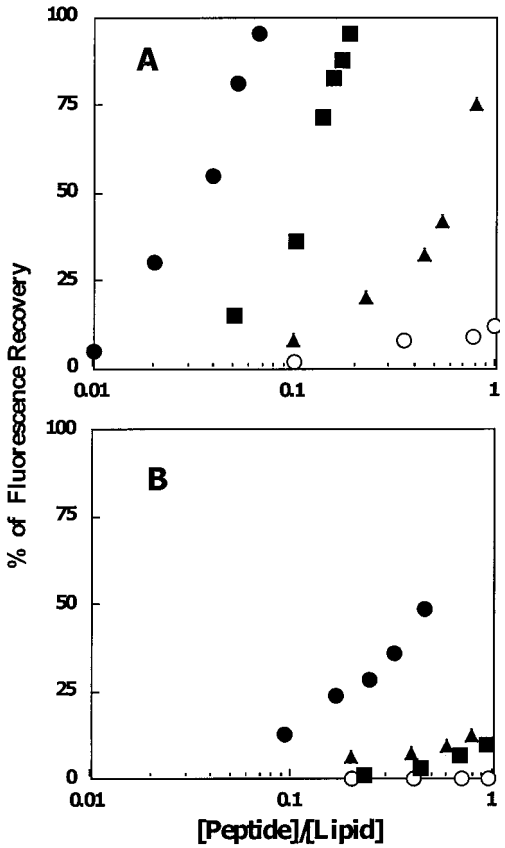

FIGURE 8: Maximal dissipation of the diffusion potential in PE/PG (A) and PC/cholesterol (B) vesicles induced by the diastereomeric peptides. Experimental conditions as in the legend to Figure 7. Designations are as follows: $K_4A_3a_4W$ (○); $K_4V_3v_4W$ (▲); $K_4I_3i_4W$ (■); $K_4L_3l_4W$ (●).

zation and decreased vesicle sizes (Figure 9B) and $K_4I_3i_4W$ induced the formation of large, fused membranes (Figure 9C). Contrary to the relatively uniform effect of the diastereomers, the corresponding parental peptides formed a mixture of large aggregates composed of micelles and fused vesicles (Figure 9D).

Electron Microscopy Visualization of Bacterial Lysis. The effect of the parental and diastereomeric peptides on the morphology of *E. coli* and *P. aeruginosa* was visualized using transmission electron microscopy. Experiments were done only when MICs were less than 70 μM. At concentrations corresponding to 60% of the MIC, significant differences in the morphology of the treated bacteria were noted. More specifically, $K_4L_3l_4W$ micellized the cell wall and membrane of both *E. coli* (Figure 10B) and *P. aeruginosa* (Figure 10E), whereas $K_4I_3i_4W$ caused an irregular disruption of large portions of the bacterial cell wall and membrane (Figure 10C). However, at the MIC, both peptides completely lysed the bacteria (data not shown). The parent K_4L_7W that formed a mixture of large aggregates composed of micelles and fused LUV vesicles (Figure 9D) caused the formation of larger blebs on *E. coli* (Figure 10F). The results of the electron microscopy studies, using a model membrane typical of *E. coli* and intact bacteria, further suggest that $K_4L_3l_4W$ and $K_4I_3i_4W$ disrupt membranes through different mechanisms.

DISCUSSION

We examined the effect of the aliphatic amino acids, Leu, Ile, Val, Ala, and Gly on the biological function, membrane binding, structure within the membrane, and mechanism of membrane disruption of linear all L-amino acid and diastereomeric amphipathic peptides. In contrast to all L-amino acid parental peptides, the diastereomers are monomeric in solution and predominantly monomers in phospholipid membranes (rhodamine quenching experiments) and within a membrane mimetic environment (Figure 3). Therefore, we could investigate direct structural changes that occurred upon transfer from water to the membrane environment and the corresponding effect on biological function.

As previously mentioned, electrostatic and hydrophobic interactions act concertedly to promote peptide-lipid association and increase membrane permeability. With most of the antimicrobial peptides tested so far, initial electrostatic binding to negatively charged membranes occurs because of the peptide's net positive charge. The hydrophobic portion of the peptide governs the subsequent stages leading to membrane permeability (see review in refs *2* and *17*). All the peptides in the present study have the same number and position of positive charges (Figure 1). Therefore, electrostatic interactions are presumably similar in all of them,

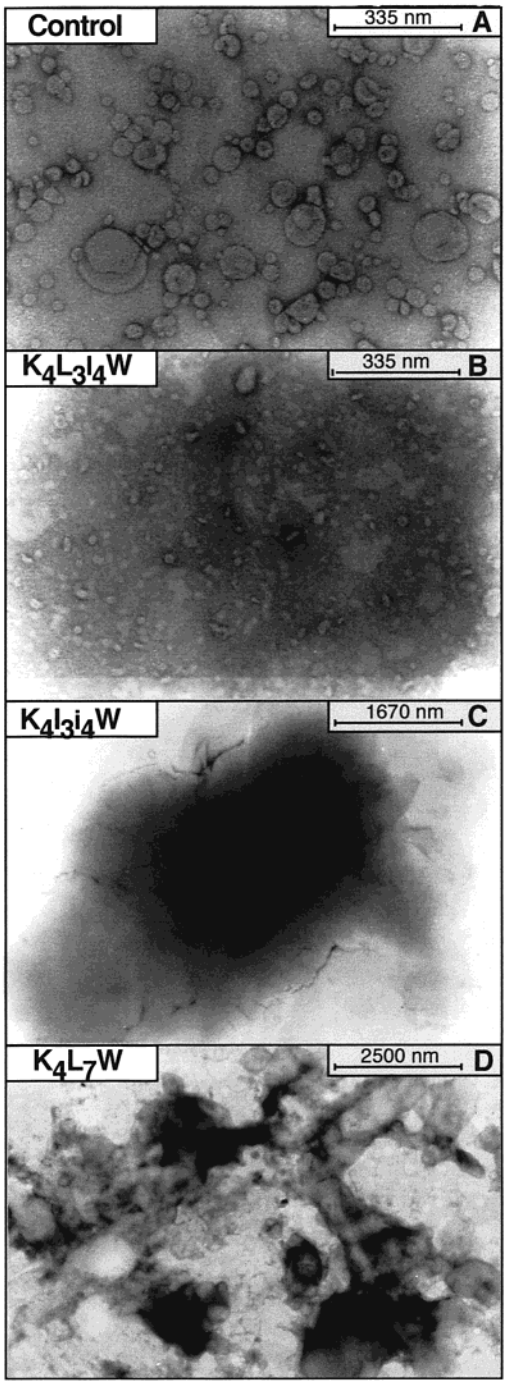

FIGURE 9: Electron micrographs of negatively stained LUV composed of PE/PG (7:3 w/w) in the absence (A), or in the presence of $K_4L_3l_4W$ (peptide:lipid molar ratio 1:25, panel B), $K_4I_3i_4W$ (peptide:lipid molar ratio 1:10, panel C), or K_4L_7W (peptide:lipid molar ratio 1:20, panel C). K_4I_7W gave similar results to K_4L_7W and is therefore not shown.

allowing us to compare the effect of hydrophobic amino acid substitution on peptide structure and function in the membrane.

Aliphatic Amino Acids Effects on Peptide Structure within the Membrane and Biological Function. The Leu-containing peptide, which is the only one that adopts a predominantly amphipathic α-helix in its all-L-form in PE/PG as revealed by using FTIR spectroscopy (Table 4) and in SDS micelles by using CD spectroscopy (data not shown), preserves a helical structure (shifted to a distorted/3_{10} helix) in its diastereomeric form. This may partially explain its high antibacterial activity (Table 2) and ability to increase membrane permeability in both the D- and the L-forms (Figures 7 and 8). The other three diastereomers, containing Ile, Val, and Ala, also adopt significant distorted helix/3_{10} helix structures, although only about half that of the diastereomeric Leu peptide. The difference in their antibacterial activity and ability to increase the permeability of the PE/PG membranes can be explained by a difference in their hydrophobicities. The relative hydrophobicities of the peptides [based on elution times using C_{18} RP-HPLC (Table 1)] also correlate with the contribution of the free energy of partitioning of the amino acids into membrane interface, which is $\Delta G = -0.56 \pm 0.04$, -0.31 ± 0.06, $+0.07 \pm 0.05$, $+0.17 \pm 0.06$, and $+0.01 \pm 0.05$ kcal/mol for Leu, Ileu, Val, Ala, and Gly, respectively (*11*, *49*). The Gly-containing peptide is an exception probably because it is unstructured when bound to the hydrophobic C_{18} aliphatic chain. The Ile- and Val-containing all L-amino acid peptides form predominantly β-sheet structures in PE/PG as revealed in the FTIR spectroscopy (Table 4) and in SDS micelles as revealed by using CD spectroscopy (data not shown). It should be noted that transmembrane peptides containing Val and Ile typically adopt a helical structure in nonpolar environments (*14*−*16*, *63*). Overall, our results reveal a correlation between the hydrophobicity of the diastereomers and an ability to form a helical structure (despite the incorporation of 30% D-amino acids) with the trends of estimated ΔG values, membrane permeability (Figures 7 and 8), and antibacterial activity (Table 2).

Mode of Increasing Membrane Permeability. We found several differences between the Leu- and the Ile-containing diastereomers that suggest a basis explaining the differences observed in their effects on vesicles and bacteria. (i) The Leu diastereomer ($K_4L_3l_4W$) did not significantly change the lipid order of PE/PG membranes, whereas a dose-dependent disruption of the acyl chain order was observed with the Ile diastereomer ($K_4I_3i_4W$, Table 5). This does not mean that $K_4L_3l_4W$ interacts with the acyl chains less than $K_4I_3i_4W$. (ii) $K_4L_3l_4W$ is more hydrophobic than $K_4I_3i_4W$ (Table 1 and ΔG binding). (iii) $K_4L_3l_4W$ is a predominantly distorted helix whereas $K_4I_3i_4W$ is ∼30% random coil. Peptide interaction with membranes to form micelles should be stronger than induction of membrane fusion. Since both peptides penetrate the vesicles to the same extent (tryptophan blue shift and bromine quenching experiments), the higher hydrophobicity and amphipathic helical structure of $K_4L_3l_4W$ may assist in stronger interactions with the membranes contributing to the formation of stable micelles (possibly bicelles). Further evidence for the involvement of amphipathic α-helical peptides in membrane micellization was observed with magainin 2 (*64*), Ac-18A-NH_2, a class A peptide (*65*), and cyclic tachyplesin I (*66*), which impose a positive curvature strain on lipid bilayers. $K_4I_3i_4W$ probably cannot act via this mechanism due the significant amount of random coil.

All L-amino acid peptides and diastereomers bind differently to zwitterionic PC/cholesterol membranes. In contrast to their high affinity to negatively charged PE/PG membranes, which results in increase in membrane permeability (Figures 7 and 8), the diastereomers bind very weakly to zwitterionic PC/cholesterol membranes. This might explain their low hemolytic activity compared to the parent L-amino acid peptides (Figure 2), since zwitterionic phospholipids are

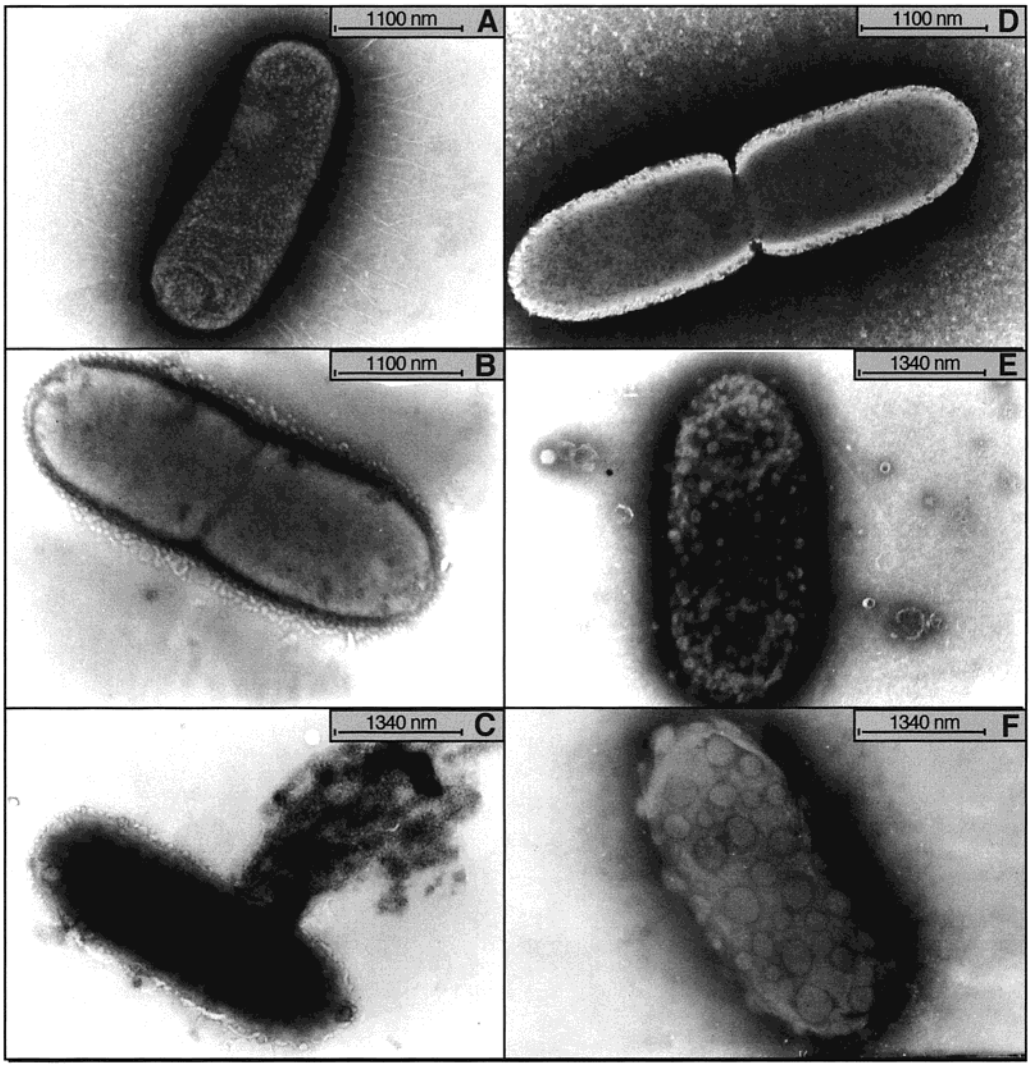

FIGURE 10: Electron micrographs of negatively stained *E. coli* and *P. aeruginosa* untreated and treated with the peptides at 60% of their MIC. (A) Untreated *E. coli*; (B) after treatment of *E. coli* with $K_4L_3l_4W$; (C) *E. coli* after treatment with $K_4I_3i_4W$; (D) untreated *P. aeruginosa*; (E) after treatment of *P. aeruginosa* with $K_4L_3l_4W$; (F) after treatment of *E. coli* with K_4L_7W.

the major component of the outer leaflet of red blood cells (*46*). The repulsion of the diastereomers from the positively charged choline group of PC may prevent penetration into the hydrophobic region of the bilayers to create an active secondary structure, as suggested for other nonhemolytic, amphipathic, helical peptides (*67*, *68*).

In summary, using model diastereomeric amphipatic helical peptides we were able to eliminate the problem of peptide aggregation. Since these diastereomeric peptides have the same sequence of hydrophobic and positively charged amino acids, their distinct binding properties and ability to increase membrane permeability can only be explained by their different hydrophobicity and secondary structure propensities in phospholipid membranes. The two main conclusions of this study are (i) a threshold of hydrophobicity and propensity to form a helical amphipathic structure are required for increasing membrane permeability and antibacterial activities, even in peptides containing ~30% D-amino acids, and (ii) increases in membrane permeability can proceed through different mechanisms. The more helical diastereomer $K_4L_3l_4W$ (predominantly α-helix in its all L-amino acid form, K_4L_7W) increases membrane permeability through micellization, while the peptide $K_4I_3i_4W$ with a low fraction of helix (predominantly aggregated β-sheets in its all L-amino acid form, K_4I_7W) hydrophobically interacts with the acyl chain region, suggestively causing membrane disruption.

REFERENCES

1. Boman, H. G. (1995) *Annu. Rev. Immun. 13*, 61−92.
2. Oren, Z., and Shai, Y. (1998) *Biopolymers 47*, 451−463.
3. Hancock, R. E., and Lehrer, R. (1998) *Trends Biotechnol. 16*, 82−88.
4. Epand, R. M., and Vogel, H. J. (1999) *Biochim. Biophys. Acta 1462*, 11−28.
5. Tossi, A., Sandri, L., and Giangaspero, A. (2000) *Biopolymers 55*, 4−30.
6. Kyte, J., and Doolittle, R. F. (1982) *J. Mol. Biol. 157*, 105−132.
7. Eisenberg, D. (1984) *Annu. Rev. Biochem. 53*, 595−623.
8. Engelman, D. M., Steitz, T. A., and Goldman, A. (1986) *Annu. Rev. Biophys. Chem. 15*, 231−353.
9. Nakai, K., Kidera, A., and Kaneshisa, M. (1988) *Protein Eng. 2*, 93−100.
10. Sharp, K. A., Nicholls, A., Friedman, R., and Honig, B. (1991) *Biochemistry 30*, 9686−9697.
11. Wimley, W. C., and White, S. H. (1996) *Nat. Struct. Biol. 3*, 842−848.

12. Thorgeirsson, T. E., Russell, C. J., King, D. S., and Shin, Y. K. (1996) *Biochemistry 35*, 1803−1809.
13. Russell, C. J., Thorgeirsson, T. E., and Shin, Y. K. (1999) *Biochemistry 38*, 337−346.
14. Deber, C. M., and Li, S. C. (1995) *Biopolymers 37*, 295−318.
15. Deber, C. M., and Goto, N. K. (1996) *Nat. Struct. Biol. 3*, 815−818.
16. Liu, L. P., Li, S. C., Goto, N. K., and Deber, C. M. (1996) *Biopolymers 39*, 465−470.
17. Castano, S., Cornut, I., Buttner, K., Dasseux, J. L., and Dufourcq, J. (1999) *Biochim. Biophys. Acta 1416*, 161−175.
18. Pouny, Y., and Shai, Y. (1992) *Biochemistry 31*, 9482−9490.
19. Shai, Y., and Oren, Z. (1996) *J. Biol. Chem. 271*, 7305−7308.
20. Oren, Z., and Shai, Y. (1996) *Biochemistry 36*, 1826−1835.
21. Wieprecht, T., Dathe, M., Schumann, M., Krause, E., Beyermann, M., and Bienert, M. (1996) *Biochemistry 35*, 10844−10853.
22. Sharon, M., Oren, Z., Shai, Y., and Anglister, J. (1999) *Biochemistry 38*, 15303−15316.
23. Hong, J., Oren, Z., and Shai, Y. (1999) *Biochemistry 38*, 16963−16973.
24. Merrifield, R. B., Vizioli, L. D., and Boman, H. G. (1982) *Biochemistry 21*, 5020−5031.
25. Gazit, E., Lee, W. J., Brey, P. T., and Shai, Y. (1994) *Biochemistry 33*, 10681−10692.
26. Kliger, Y., Aharoni, A., Rapaport, D., Jones, P., Blumenthal, R., and Shai, Y. (1997) *J. Biol. Chem. 272*, 13496−13505.
27. Greenfield, N., and Fasman, G. D. (1969) *Biochemistry 8*, 4108−4116.
28. Wu, C. S., Ikeda, K., and Yang, J. T. (1981) *Biochemistry 20*, 566−570.
29. Schagger, H., and Jagow, G. V. (1987) *Anal. Biochem. 166*, 368−379.
30. Mao, D.,and Wallace, B. A. (1984) *Biochemistry 23*, 2667−2673.
31. Oren, Z., and Shai, Y. (2000) *Biochemistry 39*, 6103−6114.
32. Surewicz, W. K., Mantsch, H. H., and Chapman, D. (1993) *Biochemistry 32*, 389−394.
33. Harrick, N. J. (1967) *Internal Reflection Spectroscopy*, Interscience, New York.
34. Ishiguro, R., Kimura, N., and Takahashi, S. (1993) *Biochemistry 32*, 9792−9797.
35. Huber, W., and Mantsch, H. H. (1991) *Biophys. J. 59*, 1261−1272.
36. Sims, P. J., Waggoner, A. S., Wang, C. H., and Hoffmann, J. R. (1974) *Biochemistry 13*, 3315−3330.
37. Shai, Y., Bach, D., and Yanovsky, A. (1990) *J. Biol. Chem. 265*, 20202−20209.
38. Bolen, E. J., and Holloway, P. W. (1990) *Biochemistry 29*, 9638−9643.
39. De Kroon, A. I., Soekarjo, M. W., De Gier, J., and De Kruijff, B. (1990) *Biochemistry 29*, 8229−8240.
40. Schiffer, M., and Edmundson, A. B. (1967) *Biophys. J. 7*, 121−135.
41. Steiner, H., Hultmark, D., Engstrom, A., Bennich, H., and Boman, H. G. (1981) *Nature 292*, 246−248.
42. Oren, Z., Lerman, J. C., Gudmundsson, G. H., Agerberth, B., and Shai, Y. (1999) *Biochem. J. 341*, 501−513.
43. Kliger, Y., Peisajovich, S. G., Blumenthal, R., and Shai, Y. (2000) *J. Mol. Biol. 301*, 905−914.
44. Lemmon, M. A., Flanagan, J. M., Hunt, J. F., Adair, B. D., Bormann, B. J., Dempsey, C. E., and Engelman, D. M. (1992) *J. Biol. Chem. 267*, 7683−7689.
45. Simmerman, H. K. B., Kobayashi, Y. M., Autry, J. M., and Jones, L. R. (1996) *J. Biol. Chem. 271*, 5941−5946.
46. Verkleij, A. J., Zwaal, R. F., Roelofsen, B., Comfurius, P., Kastelijn, D., and Deenen, L. V. (1973) *Biochim. Biophys. Acta 323*, 178−193.
47. Shaw, N. (1974) *Adv. Appl. Microbiol. 17*, 63−108.
48. Murray, D., Arbuzova, A., Hangyas-Mihalyne, G., Gambhir, A., Ben-Tal, N., Honig, B., and McLaughlin, S. (1999) *Biophys. J. 77*, 3176−3188.
49. White, S. H., and Wimley, W. C. (1998) *Biochim. Biophys. Acta 1376*, 339−352.
50. Frey, S., and Tamm, L. K. (1991) *Biophys. J. 60*, 922−930.
51. Jackson, M., and Mantsch, H. H. (1995) *Crit. Rev. Biochem. Mol. Biol. 30*, 95−120.
52. Tatulian, S. A., Biltonen, R. L., and Tamm, L. K. (1997) *J. Mol. Biol. 268*, 809−815.
53. Krause, E., Beyermann, M., Dathe, M., Rothemund, S., and Bienert, M. (1995) *Anal. Chem. 67*, 252−258.
54. Rothemund, S., Beyermann, M., Krause, E., Krause, G., Bienert, M., Hodges, R. S., Sykes, B. D., and Sonnichsen, F. D. (1995) *Biochemistry 34*, 12954−12962.
55. Dwivedi, A. M., and Krimm, S. (1984) *Biopolymers 23*, 923−943.
56. Rothschild, K. J., and Clark, N. A. (1979) *Science 204*, 311−312.
57. Goormaghtigh, E., Cabiaux, V., and Ruysschaert, J.-M. (1994) in *Subcellular Biochemistry* (Hilderston, H. J., and Ralston, G. B., Eds.) pp 329−362, Plenum Press, New York.
58. Yu, Y. G., Thorgeirsson, T. E., and Shin, Y. K. (1994) *Biochemistry 33*, 14221−14226.
59. Hirstova, K., Wimley, W. C., Mishra, V. K., G. M., A., Segrest, J. P., and White, S. H. (1999) *J. Mol. Biol. 290*, 99−117.
60. Fringeli, U. P., Gunthard, H. H. (1981) *Infrared membrane spectroscopy*, Springer-Verlag, Berlin.
61. Gazit, E., Miller, I. R., Biggin, P. C., Sansom, M. S. P., and Shai, Y. (1996) *J. Mol. Biol. 258*, 860−870.
62. Cameron, D. G., Casal, H. L., Gudgin, E. F., and Mantsch, H. H. (1980) *Biochim. Biophys. Acta 596*, 463−467.
63. Lee, S., Yoshitomi, H., Morikawa, M., Ando, S., Takiguchi, H., Inoue, T., and Sugihara, G. (1995) *Biopolymers 36*, 391−398.
64. Matsuzaki, K., Sugishita, K., Ishibe, N., Ueha, M., Nakata, S., Miyajima, K., and Epand, R. M. (1998) *Biochemistry 37*, 11856−11863.
65. Epand, R. M., Gawish, A., Iqbal, M., Gupta, K. B., Chen, C. H., Segrest, J. P., and Anantharamaiah, G. M. (1987) *J. Biol. Chem. 262*, 9389−9396.
66. Matsuzaki, K., Nakayama, M., Fukui, M., Otaka, A., Funakoshi, S., Fujii, N., Bessho, K., and Miyajima, K. (1993) *Biochemistry 32*, 11704−11710.
67. Ladokhin, A. S., and White, S. H. (1999) *J. Mol. Biol. 285*, 1363−1369.
68. Wieprecht, T., Apostolov, O., Beyermann, M., and Seelig, J. (1999) *J. Mol. Biol. 294*, 785−794.

BI0105330